The risk of scaling in Danish geothermal plants and its effect on the reservoir properties predicted by hydrogeochemical modelling

Jolanta Kazmierczak, Nicolas C.M. Marty, Rikke Weibel, Lars Henrik Nielsen, Hanne Dahl Holmslykke

Geothermics 105 (2022) 102542

Contents lists available at ScienceDirect

Geothermics

journal homepage: www.elsevier.com/locate/geothermics

The risk of scaling in Danish geothermal plants and its effect on the reservoir properties predicted by hydrogeochemical modelling

Jolanta Kazmierczak [a,*], Nicolas Marty [b], Rikke Weibel [a], Lars Henrik Nielsen [a], Hanne Dahl Holmslykke [a]

[a] Department of Geochemistry, Geological Survey of Denmark and Greenland, Øster Voldgade 10, Copenhagen K, Copenhagen 1350, Denmark
[b] Bureau de Recherches Géologiques et Minières (BRGM), France

ARTICLE INFO

Keywords:
Scaling
Barite nucleation
Hydrogeochemical modelling
Geothermal plants
Reservoir porosity changes

ABSTRACT

Injectivity problems have been observed in two of three Danish geothermal plants. The utilized geothermal reservoirs comprise sandstones of Lower Triassic and Upper Triassic – Lower Jurassic. The great variations in the formation mineralogy and the chemical composition of their brines allow for a thorough analysis of the differences in the potential risks of scaling. The key scaling processes upon injection of the cooled brines into the reservoirs were identified and changes in the reservoir porosity assessed by hydrogeochemical modelling. Scaling was predicted to be of importance only in one of the geothermal reservoirs, where barite precipitation in the near field of the injection well was identified as a potential risk and could potentially alter the reservoir porosity. Scaling induced by barite nucleation in the injection well, and precipitation and dissolution of carbonates, silicates and clays in the geothermal reservoirs are all of minor importance.

1. Introduction

Geothermal energy production utilizes the thermal energy generated and stored in the deep subsurface of the earth. In the process of geothermal energy utilization, formation water is extracted, the heat is exchanged from the water and the cooled formation water reinjected into the reservoir. Injection of the cooled formation water may lead to various clogging mechanisms in sandstone aquifers, e.g. physical, biological, chemical and air clogging, particle recombination and clay swelling (Song et al., 2020). The most common clogging mechanisms in geothermal plants are physical, biological and chemical cloggings that account for 50, 15 and 10% of the clogging cases, respectively (Song et al., 2020).

Chemical clogging is mainly induced by adverse thermochemical reactions (Song et al., 2020). Formation water in deep sedimentary basins usually contains large quantities of ions, even up to 400 g L^{-1} (Bozau et al., 2015). Changed thermodynamic conditions, in particular lowered temperature and pressure, during the geothermal energy production reduce the solubility of most minerals and increase the risk of scaling, corrosion of metal surfaces in contact with the fluids, and emission of gasses (Andritsos and Karabellas, 1991; Andritsos et al., 2002; Demir et al., 2014; Nitschke et al., 2014; Bozau et al., 2015; Wanner et al., 2017). In addition, precipitating minerals may incorporate naturally occurring radioactive nuclides and therefore may be a potential hazard to health and environment (Zhu, 2003; Nitschke et al., 2014). Some types of scaling are microbially induced precipitations (Nitschke et al., 2014).

Scaling may take place at several locations in the geothermal system, in the producing wells, surface facilities, reinjection lines, and the reservoir rocks (Demir et al., 2014; Bozau et al., 2015; Wanner et al., 2017) and may jeopardize geothermal energy production by reducing the flow in the producer and the injectivity from the injection well to the reservoir. Furthermore, precipitation of the solid phases in the reservoirs reduces porosity and permeability causing injectivity challenges (White and Mroczek, 1998; Xiao et al., 2018; Song et al., 2020). The composition of scales depends on parameters, such as formation water composition and pH, temperature and pressure in the geothermal loop, reservoir rock mineralogy and the operating conditions, e.g., the injection rates (e.g. Bozau et al., 2015; Tonkul et al., 2021). Several types of scaling minerals occur in geothermal plants, such as carbonates (Andritsos et al., 2002; Demir et al., 2014; Oliveira et al., 2019), barite (Bozau et al., 2015), silicates and clays (Andritsos et al., 2002; Smith and Carroll, 2016), heavy metal sulfides (Andritsos et al., 2002; Demir et al., 2014; Tonkul et al., 2021), metal hydroxides (Song et al., 2020) and

* Corresponding author.
E-mail address: jka@geus.dk (J. Kazmierczak).

https://doi.org/10.1016/j.geothermics.2022.102542
Received 7 October 2021; Received in revised form 26 July 2022; Accepted 3 August 2022
Available online 13 August 2022

metallic lead (Laier et al., 2015a, 2015b, 2015c, 2015d; Olivarius et al., 2018).

Minerals likely to precipitate or dissolve under certain conditions can be identified based on the saturation index (SI) defined as (Appelo and Postma, 2005):

$$SI = \log\left(\frac{IAP}{K}\right) \tag{1}$$

where: IAP is the ion activity product derived from water analysis, and K is the thermodynamic equilibrium constant for the mineral. Theoretically, a mineral precipitates from solution if the SI is positive. Since equilibrium constants are temperature and pressure dependant, a solution may change saturation state from subsaturated to supersaturated, or vice versa, upon changes in temperature and pressure (Appelo and Postma, 2005; Tonkul et al., 2021). Even if a solution is supersaturated with a certain mineral, the precipitation of significant amounts of minerals may depend on the reaction kinetics. Thus, the precipitation rate may be too slow for mineral precipitation to take place in the installations of a geothermal plant (Carroll et al., 1998; Ganor et al., 2005; Appelo and Postma, 2005; Hsu, 2006; Fritz and Noguera, 2009). Therefore, consideration of the reaction kinetics, especially for phases with fast precipitation and dissolution rates, is important when studying scaling in geothermal plants (Zhen-Wu et al., 2016; Cazenave et al., 2020). However, hydrogeochemical models for scaling do not always include reaction kinetics (Bozau et al., 2015).

In Denmark, three geothermal plants (Margretheholm, Sønderborg and Thisted) have been operating to produce heat for district heating. However, the two first mentioned have experienced injectivity problems and occasionally stopped operation. It has been suggested that the injection problems in Margretheholm are mainly caused by precipitation of metallic lead due to galvanic corrosion (Laier, 2015a, 2015b, 2015c). The galvanic corrosion depends on steel composition, salinity of fluid, pH, turbulent flow etc. (Bozau et al., 2015; Ng et al., 2018). Application of corrosion inhibitors was tested in Margretheholm, though the effect was not thoroughly verified (Laier, pers. comm. 2019). Several causes for the injection problems have also been proposed in Sønderborg, including sulphate reduction resulting in zinc- and lead-sulphide precipitates and possibly biofilm formation (Laier, 2016).

The objectives of this study are therefore to: (1) assess the risk of non-corrosion induced scaling in the Danish geothermal plants considering the reaction kinetics for the minerals selected based on the brine chemistry, reservoir mineralogy and reaction rates, and (2) simulate the effect of the long-term geothermal plant operation and scaling on the reservoir properties. The risk of corrosion and operational problems, such as biofilm formation etc. are not addressed further here as these challenges cannot be predicted or addressed from the geochemical modelling. The hydrogeochemical modelling was based on the composition of reservoir sandstone and brine chemistry that significantly differ for the three geothermal plants, Margretheholm, Sønderborg and Thisted. Hence, the variations in the formation mineralogy, petrography and in the chemical composition of the brines allow for a thorough analysis of the differences in the potential risks of scaling.

2. Site description and methods

2.1. Site description

2.1.1. Margretheholm geothermal plant

In the Margretheholm geothermal plant, the water flows from the production well through a bag filter, heat exchanger, membrane filter, and to the injection well. The middle part of the screen in both the production and the injection well, is at a depth of approximately 2570 m, at which depth the reservoir temperature and pressure are 72±3 °C and 286 bar, respectively (Balling et al., 2019; Fuchs et al., 2020). After cooling in the heat exchangers, the injection water temperature is approximately 20 °C. Reservoir modelling based on the production and injection data indicates that the cold front extends 300 m from the injection well into the reservoir (Fig. 1; Balling et al., 2019). The capacity of the plant is 230 $m^3\ h^{-1}$, but in recent years the typical production has been 130 $m^3\ h^{-1}$, intersected by regular production stops due to the injectivity problems.

The reservoir is in the Lower Triassic Bunter Sandstone Formation, which was deposited in an arid climate mainly from braided streams and aeolian activity (Clemmensen, 1985; Olsen, 1987; Olivarius and Nielsen, 2016). The mineralogical composition of the Bunter Sandstone Formation from the Margretheholm area has been evaluated from cuttings samples by automated mineralogical quantification (Mineralscan). The Bunter Sandstone Formation consists here mainly of quartz (57 vol %), abundant K-feldspar (25 vol%) and albite (5 vol%; Olivarius et al., 2018). Rock fragments are not identified by the Mineralscan method but are typically common in the Bunter Sandstone Formation (Weibel and Friis, 2004; Olivarius and Nielsen, 2016). Heavy minerals are rare (< 1 vol%), and thus comparably low for the Bunter Sandstone Formation elsewhere in Denmark. The cementing phases are mainly calcite (4 vol %), dolomite (3 vol%) and rare clay minerals. An average porosity of 22% has been interpreted from petrophysical logs, and corresponding permeabilities of 300 mD have been estimated from a general porosity to permeability relationship (Vosgerau et al., 2015a; Kristensen et al., 2016).

2.1.2. Sønderborg geothermal plant

The Sønderborg geothermal plant consists of a production well with a middle part of the screen at a depth of approximately 1225 m., bag filters, heat exchangers, membrane filters and an injection well with a middle part of the screen at approximately 1180 m (Balling et al., 2019). The plant is in production only in the winter season with a variable production rate (70 $m^3\ h^{-1}$ to 120 $m^3\ h^{-1}$). The reservoir temperature and pressure at a depth of 1300 m are 49±3 °C and 140 bar, respectively, and after cooling in the heat exchangers the injection water temperature is approximately 15 °C (Balling et al., 2019). According to the reservoir modelling results (Balling et al., 2019) the cold front extends 150 m from the injection well into the reservoir (Fig. 1) based on the production and injection data.

The reservoir is in the Upper Triassic–Lower Jurassic Gassum Formation, which was deposited under a humid climate in paralic and marine depositional environments (Nielsen, 2003). The Gassum Formation at Sønderborg contains abundant quartz (up to 56–57 vol%), muscovite (22 vol%), minor amounts of K-feldspar (3–4 vol%) and albite (1–2 vol%) and rare heavy minerals (< 1 vol%). Cementing phases comprise calcite (8–9 vol%), pyrite and anatase (< 1 vol%). Rare to abundant kaolinite (2–18 vol%) may comprise both clay clasts and cementing phases. The reservoir has a porosity of 28% calculated from petrophysical logs and an estimated permeability of 2800 mD (Vosgerau

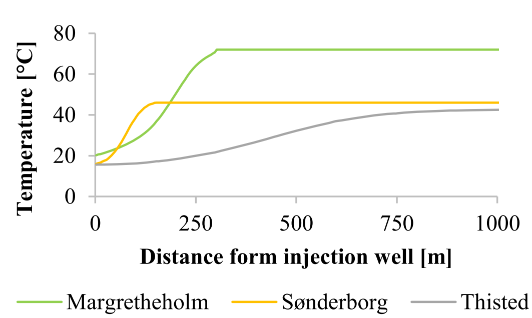

Fig. 1. Temperature gradients in the reservoirs at Margretheholm, Sønderborg and Thisted in 2015, 2018 and 2013, respectively modelled by Balling et al. (2019) and Fuchs et al. (2020). The year corresponds to the end point of the 1D and 2D axisymmetric simulation period. The temperature data were used in the 1D simulations of inflow of the cooled brines into the geothermal reservoirs as the REACTION TEMPERATURE term in PHREEQC ver.3.

et al., 2015b).

2.1.3. Thisted geothermal plant

The Thisted geothermal plant was established in 1984 and is the first geothermal plant constructed in Denmark. At the time of the data collection for this study the plant included a production well at a 1290 m depth, bag filters, heat exchangers, membrane filters and an injection well at a 1240 m depth. However, recently a new injection well to 1240 m depth was drilled to assist the initial well. Reservoir temperature and pressure at 1290 m are 43±3 °C and 140 bar, respectively, and the injection water temperature is approximately 16 °C (Balling et al., 2019). The plant is closed during the summer, from April to October and operates the rest of the year continuously with a median production rate of 95 $m^3 h^{-1}$ and the highest production rates up to 278 $m^3 h^{-1}$ in 2005. Reservoir modelling results indicate that the cold front extends 800 m from the injection well into the reservoir (Fig. 1; Balling et al., 2019).

The reservoir is the Upper Triassic–Lower Jurassic Gassum Formation, which was deposited under a humid climate in fluvial, lagoonal, tidal and shoreface depositional environment in this part of the basin (Nielsen, 2003). The Gassum Formation in the Thisted area consists of quartz dominated (50–77 vol%) sandstones with some albite (6–18 vol %) and K-feldspar (4–14 vol%). The major cementing phases are siderite (up to 22 vol%), calcite (up to 4 vol%), pyrite (up to 5 vol%), kaolinite (up to 3 vol%) and illitic clays (up to 1 vol%). The upper shoreface and fluvial–estuarine reservoir sandstones in the Thisted-3 core have average porosities of 31.3% (σ: 3.3%) and 32.7% (σ: 5.1%), respectively. Porosity and permeability values up to 40% and 1500 mD respectively have been documented from core plug measurements (Weibel et al., 2017b).

2.2. Reservoir mineralogy, water sampling and analysis

Reservoir mineralogy used in the hydrogeochemical modelling was obtained by an automated mineralogical quantification (Mineralscan) of the cutting samples in Margretheholm (2557.5 m) and Sønderborg (1990.0 m), and a core from Thisted (1222.8 m). The mineral content (Olivarius et al., 2018), corrected from porosity, is summarized in Table 1.

In order to determine the composition of solutions used for geochemical modelling water samples from the geothermal plants were collected during the operation in 2017. Hot formation water samples were collected at the well heads of the production wells, and cooled formation water was sampled prior to the injection into the reservoir. Sampling was facilitated through the taps mounted on the production line. The geothermal brine was filtered through a 0.45 µm membrane filter and split into two separate polyethylene vials. Samples for cation analysis were preserved with 1 vol% of 7 M HNO_3 and kept refrigerated. Sodium (Na), calcium (Ca), magnesium (Mg) and potassium (K) were determined by ICP–MS (PerkinElmer Elan6100DRC Quadrupol) with a standard deviation of 3–15% depending on the element. Silica (Si), iron (Fe(II)) and trace elements were determined by ICP-MS (PerkinElmer Elan 6100DRC, Elan software version 3.3) with a detection limit of 0.001–5 mg L^{-1} depending on the element. Samples for anion analysis, chloride (Cl^-) and sulphate (SO_4^{2-}), were frozen until IC analysis (Metrohm IC, 819 detector, column Metrosep A sup. 5–150/4.0) with a quantification limit of 0.05 mg L^{-1}.

2.3. Geochemical model description

2.3.1. Speciation calculations

The quality of the chemical analysis was checked and the saturation state (Eq. (1)) of the formation waters before and after cooling with respect to relevant minerals was examined using speciation calculations in PHREEQC ver.3 (Parkhurst and Appelo, 2013). The results of the speciation calculations were used to distinguish the chemical processes that are likely to take place upon cooling of the formation waters and injection of the cooled brines into reservoirs at the geothermal plants. Considering the high ionic strengths of the formation waters (Section 3.1), the Pitzer thermodynamic database (*pitzer.dat*) was used.

2.3.2. Potential precipitation and dissolution of minerals in the reservoirs

Potential dissolution and precipitation of minerals in the reservoirs upon injection of the cooled formation water and their influence on the reservoir porosity was assessed by two-dimensional (2D) axisymmetric reactive transport modelling using MARTHE-PHREEQC and *pitzer.dat* (Parkhurst and Appelo, 2013; Thiéry, 2015). The input data were solid composition (Table 1), water chemistry (Table 2) and flow rate recorded in the geothermal plants. Several minerals relevant for the geothermal reservoirs studied (e.g. aluminium (Al) bearing minerals, Table 1) are absent in *pitzer.dat* that provides more accurate results for brines with a high ionic strength. Thus, to address these solid phases, one-dimensional (1D) horizontal models using *phreeqc.dat* were constructed. *Phreeqc.dat* is based on the Debye-Hückel theory, which provides the most accurate results for low-saline solutions. With an increasing ionic strength, the certainty of the results decreases (Zhen-Wu et al., 2016). Thus, possible discrepancies caused by an execution of the models using the Debye--Hückel theory instead of Pitzer equations were evaluated by comparison of saturation indices for the key solid phases and activity coefficients of the key dissolved ions calculated using both, *phreeqc.dat* and *pitzer.dat* prior to the run of 1D transport models.

Flow of fluid through a saturated porous medium is described by Darcy's law (Zheng and Bennett, 2002):

$$q = \frac{Q}{A} = -K\frac{dH}{dL} \tag{2}$$

where q is Darcy velocity, Q is volumetric flow rate through an area (A), K is hydraulic conductivity and dH is a hydraulic gradient along the distance (dL). Chemical transport is governed by the advection-

Table 1
Mineralogy of the reservoirs in the geothermal plants used as an input for the modelling. The mass fraction is corrected from porosity. Muscovite and chlorite origin mainly from the mudstone inserts.

	Mineral	Mass fraction [%]		
		Margretheholm	Sønderborg	Thisted
Assumed unreactive in the 2D axisymmetric models*	Calcite	3.6	5.1	0.01
	Dolomite	2.8	0.02	0
	Quartz	56.4	57	65.4
	Albite	6.1	0.9	17.2
	Chlorite	7.2	3.9	0
	Illite	0.02	0.02	0
	Kaolinite	0.1	6.0	3.3
	K-feldspar	22.9	2.1	13.2
	Muscovite	0.7	22	0.7

* The solid phases assumed to be unreactive in the 2D axisymmetric models comprise Al-bearing clays and silicates that are absent in *pitzer.dat* and therefore cannot precipitate or dissolve in the model. The conservative mass fraction of these minerals was however used in the estimation of the reservoir porosity.

Table 2
Chemical composition of the brines in the geothermal plants before and after cooling.

	Margretheholm		Sønderborg		Thisted	
	Well head production well	After cooling	Well head production well	After cooling	Well head production well	After cooling
Temp (°C)	72	20	46	16	43	16
pH	5.6	5.7	6.2	6.5	5.9	6.2
	(mg L^{-1})	(mg L^{-1})	(mg L^{-1})	(mg L^{-1})	(mg L^{-1})	(mg L^{-1})
Na (±1.72%)	53,974	53,864	55,249	55,443	51,882	51,914
Ca (±2.58%)	20,505	20,483	3899	3918	6909	6881
Mg (±3.66%)	2938	2914	1101	1093	1564	1492
K (±7.05%)	636	667	219	218	248	193
Ba (±0.1 mg L^{-1})	17.2	15.6	0.8	0.7	18	17.5
Sr (±2.5 mg L^{-1})	725	706	193	198	370	388
Cl^- (±2.13%)	133,963	132,877	97,149	96,228	98,642	98,582
SO_4^{2-} (±5.24%)	230	222	729	737	86	86
HCO_3^-	30	30	60	62	45	45
Br (±2.61%)	814	879	219	222	314	317
Si (±1 mg L^{-1})	5.6	5.7	5.7	4.6	4.7	4.9
Fe(II) (±1.1 mg L^{-1})	n.d.	n.d	6	12	8	19
Mn (±0.1 mg L^{-1})	17	17	6	6	15	15
Pb (±0.04 mg L^{-1})	0.6	0.01	0.01	0.01	0.01	0
Zn (±0.1 mg L^{-1})	3.7	2.6	0.14	0.5	1	0.05

dispersion equation (Zheng and Bennett, 2002):

$$\frac{dc}{dt} = -v\frac{dc}{dL} + D_L\frac{d^2c}{dL^2} - \frac{dq}{dt} \quad (3)$$

where: c is the solute concentration in water, t is time, v is pore water flow velocity, L is distance, q is the solute concentration in the solid phase, and D_L is hydrodynamic dispersion coefficient. The latest is calculated from (Zheng and Bennett, 2002):

$$D_L = D_e + \alpha_L v \quad (4)$$

where D_e is the effective diffusion coefficient and α_L the dispersivity. The coupling of the governing flow and transport equations in the models was sequential, meaning that at each time step the velocity field was first computed in the entire domain. Then, all dissolved substances and heat were transported, and geochemical reactions computed in the temperature field.

The 1D models consisted of a 1-kilometre-long horizontal column and a cell length of 5 m. It was assumed that the column is placed at the bottom of the injection well, perpendicular to the screen. The 1D columns were flow through columns with constant flux rates at the column ends. Flow rates were estimated from the injection rates and reservoir porosities. Injection rates in 1D simulations varied between 70 and 130 m^3 h^{-1} in Sønderborg and were set at an average fixed value of 150 m^3 h^{-1} in Margretheholm and 95 m^3 h^{-1} in Thisted geothermal plants. Diffusion coefficient equalled 1.5 × 10^{-10} m^2 s^{-1}. Pressures in the reservoirs were set to 286 bar in Margretheholm, and 140 bar in Sønderborg and Thisted. Temperature gradients observed from the injection wells into the reservoirs were maintained using the REACTION_TEMPERATURE module in PHREEQC ver.3 (Parkhurst and Appelo, 2013), assigning fixed temperatures along the 1D columns in accordance with the simulated temperature profiles (Fig. 1; Balling et al., 2019). 1D PHREEQC simulations were simplified and the heat transport was not considered.

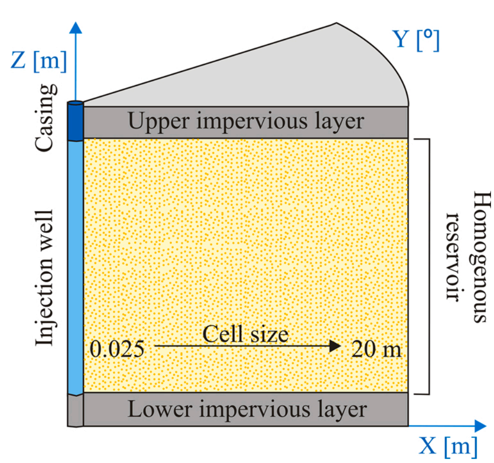

Fig. 2. Schematic representation of geometry applied to simulate precipitation and dissolution processes in the geothermal reservoirs with MARTHE-PHREEQC.

Geothermal reservoirs in the 2D axisymmetric models were represented by a single, homogenous layer with an injection well in the centre of the grid (Fig. 2). The mesh was radial with X, Y, and Z coordinates coinciding with the radius, angle, and layer of the model, respectively. The mesh size in X direction was 2.5 cm at the injection well and increased progressively up to 20 m with distance. The vertical model boundaries were set as transient flow rates estimated from hourly flow rates at the geothermal plants and reservoir porosities. Time steps in the calculations were a function of the flow rates and ranged from 1 day at 0 m^3 h^{-1} to 13.3 s at 278 m^3 h^{-1}. The diffusion coefficient was set to 1.5 × 10^{-10} m^2 s^{-1}. Top and bottom impermeable clay layers were modelled as no flow boundaries. However, an analytical solution of thermal conduction perpendicular to the reservoir (Vinsome and Westerveld, 1980) was assigned to these layers to simulate the heat transfer. The analytical solution avoids the vertical discretization of the clay layers, reduces the number of meshes in the model, and thereby the computation time. Initial temperature in the reservoirs was 72 °C at Margretheholm, 49 °C at Sønderborg and 43 °C at Thisted. The volumetric heat capacity of minerals equalled 2 × 10^6 J m^{-3} $°C^{-1}$. Heat capacity of water was 4185 J kg^{-1} $°C^{-1}$. Thermal conductivities of minerals and water were set as 2.5 and 0.6 W m^{-1} $°C^{-1}$, respectively.

Both the Bunter Sandstone Formation and the Gassum Formation show lateral and vertical variations related to depositional processes, and the reservoir quality of the two formations varies with lithology, mineralogy, grain size and diagenesis (Weibel et al., 2020). Therefore, efforts in previous studies focused toward interpreting and predicting sandstone porosity based on depositional, climatic and geochemical models (Olivarius et al., 2018; Kristensen et al., 2016; Weibel et al., 2017a, 2017b; Hjuler et al., 2019; Nielsen et al., 2019). At the three geothermal plants investigated here, the production and injection wells are completed with screens and perforations in carefully selected and short intervals of the heterogenous formations where porous sandstones prevail according to analysis of the available well-logs. Thus, for the 1D and 2D axisymmetric simulations, porosity of the selected reservoir sections was assumed to be homogenous and equalled 20% in Margretheholm, and 30% in Sønderborg and Thisted based on estimations from petrophysical logs (Vosgerau et al., 2015a, 2015b; Kristensen et al., 2016) and core plug measurements of the sandstones from the Thisted-3 core (Weibel et al., 2017b). Although there are low porosity and permeability zones due to heterolithic bedded sediments, the main reservoir is interpreted to be upper shoreface or fluvial-estuarine sandstones, which are characterized from the Thisted-3 core by having relatively uniform porosities.

Solutions injected in 1D and 2D axisymmetric models were equilibrated with calcite and dolomite, and aqueous solutions in the reservoirs were equilibrated with solid phases in the reservoirs (Table 1) and minerals for which they showed supersaturation or equilibrium state (Section 3.1), if they were available in the database. Thus, 2D axisymmetric models using *pitzer.dat* included calcite, dolomite, barite, celestite, gypsum, quartz and amorphous silica. Minerals absent in *pitzer.dat* were considered as unreactive phases (Table 1). This simplification mainly concerns mineral phases that are less likely to precipitate from a kinetic point of view (Palandri and Kharaka, 2004). 1D models using *phreeqc.dat* additionally included albite, chlorite, illite, kaolinite, K-feldspar and muscovite (Table 1). Major chemical reactions addressed in geochemical modelling are summarized in Table 3.

Application of the kinetic expressions for all mineral phases would require a large computational effort and could lead to the acceptance of numerical errors (Konikow, 2010). Thus, it is recommended to keep the transport models relatively simple and to use them to test and improve the conceptual understanding of the system (Konikow, 2010). Therefore, most of the solid phases were modelled in 1D and 2D axisymmetric simulations as the equilibrium phases (Table 3). Barite precipitation is the most likely process in the geothermal plants (Section 3.1) and was simulated using a kinetic law based on the transition state theory (TST) of Lasaga (1981). Applied kinetic parameters are from Zhen-Wu et al. (2016). To estimate the reactive surface area of barite in the reservoir, a sensitivity analysis has been carried out in the MARTHE-PHREEQC model by increasing the surface from 1×10^{-5} to 5×10^{-5} m^2 g^{-1} using the data for Margretheholm geothermal plant.

Initial amounts of the minerals present in the reservoirs per litre of aqueous solution in 1D models and per litre of rock in 2D axisymmetric models were calculated based on the results of Mineralscan (Table 1). Quartz precipitation is unlikely at the geothermal plants. Quartz did not precipitate in the geothermal reservoirs at temperatures < 350 °C and depths shallower than 2 km (White and Mroczek, 1998), and at temperatures < 100 °C amorphous silica may form (Rimstidt and Barnes, 1980; Tonkul et al., 2021). Thus, only dissolution of quartz and precipitation of amorphous silica were allowed in the model. For the remaining phases both precipitation and dissolution could take place.

The models were run for the period 2004–2015 (10.6 years) for Margretheholm geothermal plant, 2013–2018 (4.6 years) for Sønderborg geothermal plant (full operation period at the time of the modelling study), and 2000–2013 (12.9 years) for Thisted geothermal plant. Production at Margretheholm significantly decreased after 2015 due to the injectivity problems, and thus this period was not included in the simulation. Simulation time for the Thisted geothermal plant corresponds to the period with available flow rate data. Extension of the simulation time in Thisted would not influence conclusions of the study, as a significant precipitation of minerals and therefore a reduction in the reservoir porosity were not predicted by geochemical modelling (Section 3). Furthermore, no injectivity problems were experienced in Thisted geothermal plant during over 30 years of the plant operation.

2.3.3. Barite nucleation in the injection well

Barite formation kinetics are fast and barite scaling can take place already in the injection well (Bozau et al., 2015; Zhen-Wu et al., 2016). The importance of nucleation in the scale formation in a flow through tube was shown by Lu et al. (2020). Therefore, barite nucleation in the injection wells was modelled in 1D using the barite nucleation code developed in PHREEQC ver.3 (Parkhurst and Appelo, 2013) by Dideriksen et al.. The model is based on the extended *pitzer.dat* database (in prep. Dideriksen et al., 2022) and barite kinetic rates described in Zhen-Wu et al. (2016). It is assumed that barite is not present initially in the system to enable the seeded growth, and the nucleation modelling is based on the classical nucleation theory and encompasses energy barriers for nucleation, which translate into nucleation rate, etc. The nuclei then grow based on rates for crystal growth, evolving their surface area. The classical nucleation theory represents well the process of barite nucleation that takes place in the flowing tube (Lu et al., 2020).

The model set up by Dideriksen et al. (2022) is slightly simplified and assumes that the barite saturation state is constant. Furthermore, the model does not include the concept of induction time which stems from batch experiments where two solutions are mixed to induce supersaturation (He et al., 1995), as it is uncertain how this concept translates to a flow through system like a well. The well surface in a flow through system is for longer time spans exposed to the same type of solution. At the surfaces, the organization of the ions or liquid-liquid separation could take place, albeit such processes might not have taken place in the bulk solution. Thus, it is not obvious that a straightforward translation exists, like that proposed by He et al. (1995), where nucleation is suppressed if the induction time for nucleation is longer than the residence time of the water in a well.

Each of the injection wells was divided into 10 cells of an equal length. The density of the sites available for barite nucleation at the wells depended on the well diameter. The nucleation process was simulated for one week of a cooled brine injection with rates 150, 130 and 95 m^3 h^{-1} for Margretheholm, Sønderborg, and Thisted, respectively. A linear pressure gradient was assumed. The pressure equalled

Table 3
Minerals and reactions included in geochemical modelling.

Mineral	Chemical equation	Precipitation/Dissolution	Kinetic/Equilibrium
Albite*	$NaAlSi_3O_8 + 8\ H_2O = Na^+ + Al(OH)_4^- + 3\ H_4SiO_4$	Dissolution	Equilibrium
Barite	$BaSO_4 = Ba^{+2} + SO_4^{-2}$	Precipitation/Dissolution	Kinetic
Calcite	$CaCO_3 = CO_3^{-2} + Ca^{+2}$	Precipitation/Dissolution	Equilibrium
Celestite	$SrSO_4 = Sr^{+2} + SO_4^{-2}$	Precipitation/Dissolution	Equilibrium
Chlorite*	$Mg_5Al_2Si_3O_{10}(OH)_8 + 16\ H^+ = 5\ Mg^{+2} + 2\ Al^{+3} + 3\ H_4SiO_4 + 6\ H_2O$	Precipitation/Dissolution	Equilibrium
Dolomite	$CaMg(CO_3)_2 = Ca^{+2} + Mg^{+2} + 2\ CO_3^{-2}$	Precipitation/Dissolution	Equilibrium
Gypsum	$CaSO_4{:}2H_2O = Ca^{+2} + SO_4^{-2} + 2\ H_2O$	Precipitation/Dissolution	Equilibrium
Illite*	$K_{0.6}Mg_{0.25}Al_{2.3}Si_{3.5}O_{10}(OH)_2 + 11.2\ H_2O =$ $0.6\ K^+ + 0.25\ Mg^{+2} + 2.3\ Al(OH)_4^- + 3.5\ H_4SiO_4 + 1.2\ H^+$	Precipitation/Dissolution	Equilibrium
Kaolinite*	$Al_2Si_2O_5(OH)_4 + 6\ H^+ = H_2O + 2\ H_4SiO_4 + 2\ Al^{+3}$	Precipitation/Dissolution	Equilibrium
K-feldspar*	$KAlSi_3O_8 + 8\ H_2O = K^+ + Al(OH)_4^- + 3\ H_4SiO_4$	Dissolution	Equilibrium
Muscovite*	$KAl_3Si_3O_{10}(OH)_2 + 10\ H^+ = K^+ + 3\ Al^{+3} +$ $3\ H_4SiO_4$	Dissolution	Equilibrium
Quartz	$SiO_2 + 2\ H_2O = H_4SiO_4$	Dissolution	Equilibrium

* Minerals included only in 1D PHREEQC simulations.

10 bar in the first cell. A pressure of 10 to 15 bar was observed at the well heads in the geothermal plants during the sampling in 2017. Pressure at the well bottom was set to 286 bar in Margretheholm, and 140 bar in Sønderborg and Thisted. Transported solutions had the temperature and composition of the cooled brines (Table 2).

3. Results and discussion

3.1. Chemical composition of the formation water

The formation water in the geothermal plants is very saline with ionic strengths of 3.4–5.8 mol kgw^{-1} (Table 2). The results of speciation calculations using PHREEQC ver.3 indicate charge balance errors of up to 5.2%. Charge balances up to 5% are generally accepted for dilute samples (Appelo and Postma, 2005) and the data from the three geothermal plants were therefore assumed to be robust considering the high salinity of the samples. Differences in ion concentrations between production and injection wells are either within the analytical error (Table 2) or a result of chemical processes taking place upon brine cooling.

Evaluation of the saturation state of the cooled formation water revealed the risk of barite precipitation in the three geothermal plants (Fig. 3) despite the differences in the brine chemistry (temperature, pH and Ba^{2+} and SO_4^{2-} concentrations), Table 2. In line with the results of Holmslykke et al. (2019), the formation water in the reservoirs was in equilibrium with calcite, quartz and barite, and additionally with celestite and dolomite in Margretheholm and Sønderborg (Fig. 3). Upon cooling, the geothermal brine became supersaturated with respect to barite in all investigated geothermal plants and additionally with quartz in Sønderborg and Thisted and calcite and dolomite in Margretheholm (Fig. 3). Changes in Pb and Zn concentration may be caused by precipitation of metals due to galvanic corrosion in the geothermal loop (Laier, 2015a; 2015b; 2015c). However, this process was not a subject of our study.

The low brine temperature after heat extraction (16 to 20 °C) and slow reaction kinetics at these temperatures were clearly unfavourable for quartz precipitation (Rimstidt and Barnes, 1980). In contrast, the precipitation of barite is fast even at low temperatures, and the precipitation rate is not significantly affected by high concentrations of aqueous Ca, Mg and Sr (Zhen-Wu et al., 2016). Hence, barite precipitation could not be excluded during cooling of the fluid through the geothermal loops and in the cooled parts of the reservoir.

The geothermal loops are sealed from gas influx and outflux, and therefore the system is closed and pCO_2 in brines is a product of hydrogeochemical processes in the reservoirs. The brine in the Margretheholm reservoir was in equilibrium with calcite and dolomite, while the cooled brine was supersaturated with respect to carbonates (Fig. 3). The fluid cooling without CO_2 degassing increases the solubility

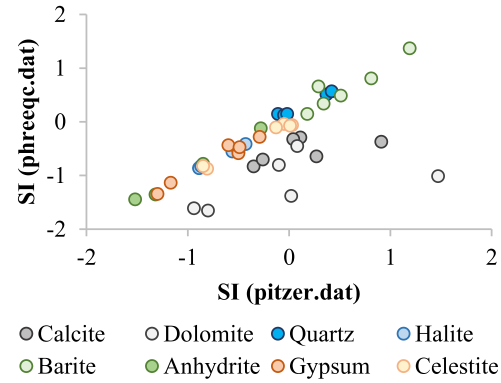

Fig. 4. Saturation indices of the formation water and cooled brines calculated with the *pitzer.dat vs. phreeqc.dat*.

of the carbonate minerals and prevents their precipitation (Appelo and Postma, 2005; Wanner et al., 2017; Song et al., 2020; Tonkul et al., 2021). Therefore, the supersaturation of carbonate minerals in the cooled brine in Margretheholm was more likely an effect of CO_2 degassing during the sampling of the cooled formation water that resulted in an increase in pH (Table 2) and in the saturation indices with respect to calcite and dolomite (Fig. 3). Trémosa et al. (2014) demonstrated that calculations using the B-dot model, an extension of the Debye-Hückel activity model, failed in reproducing simple mineral solubilities for NaCl salinities higher than 1 mol kgw^{-1} even though the saline waters are of NaCl type. In contrast, calculations using the Pitzer interaction model clearly improved experimental data reproduction and allowed mineral solubility to be captured as a function of salinity in a relatively good manner (Trémosa et al., 2014). The ionic strength of the brines ranged 3.4–5.8 mol kgw^{-1} and discrepancies were observed between saturation indices and activity coefficients calculated based on *phreeqc.dat* or *pitzer.dat* (Figs 4 and 5). Thus, *pitzer.dat* was used in a 2D axisymmetric model to predict geochemical processes in the reservoir. However, the major part of saturation indices and activity coefficients in the formation water and cooled brines from the geothermal plants predicted using *phreeqc.dat* fitted well to the calculation results from *pitzer.dat* (Figs. 4 and 5). Exceptions were carbonates (calcite and dolomite) and cations (Ca, Mg, Ba, Sr) that had slightly lower SI and activity coefficients predicted using *phreeqc.dat* (Figs. 4 and 5). Therefore, *phreeqc.dat* was applied in the 1D model in order to assess precipitation and dissolution of the Al-bearing minerals and silicates in the geothermal plants, as *pitzer.dat* does not include these phases. However, the results for the 1D model have an increased uncertainty due to the application of *phreeqc.dat* in modelling of brines with a high ionic strength.

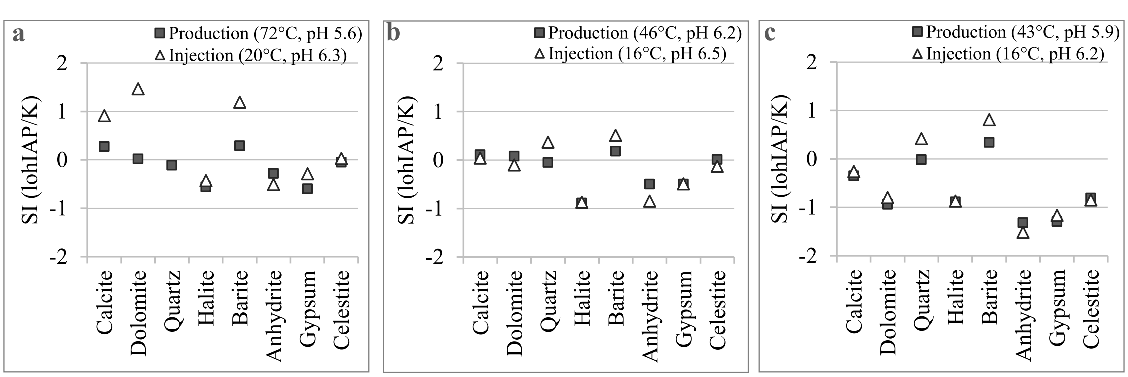

Fig. 3. Saturation indices of the formation water and cooled brines at Margretheholm (a), Sønderborg (b) and Thisted (c) geothermal plants calculated using PHREEQC ver. 3 and pitzer.dat.

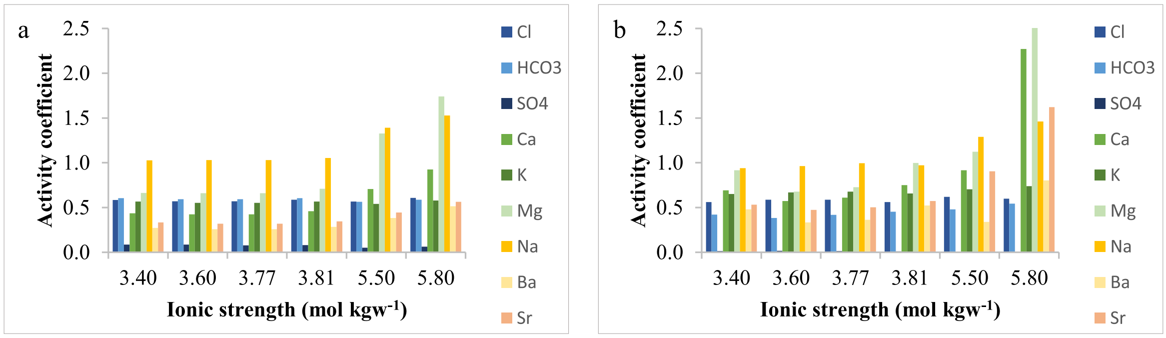

Fig. 5. Ionic strength *vs.* activity coefficients calculated using *phreeqc.dat* (a) and *pitzer.dat* (b).

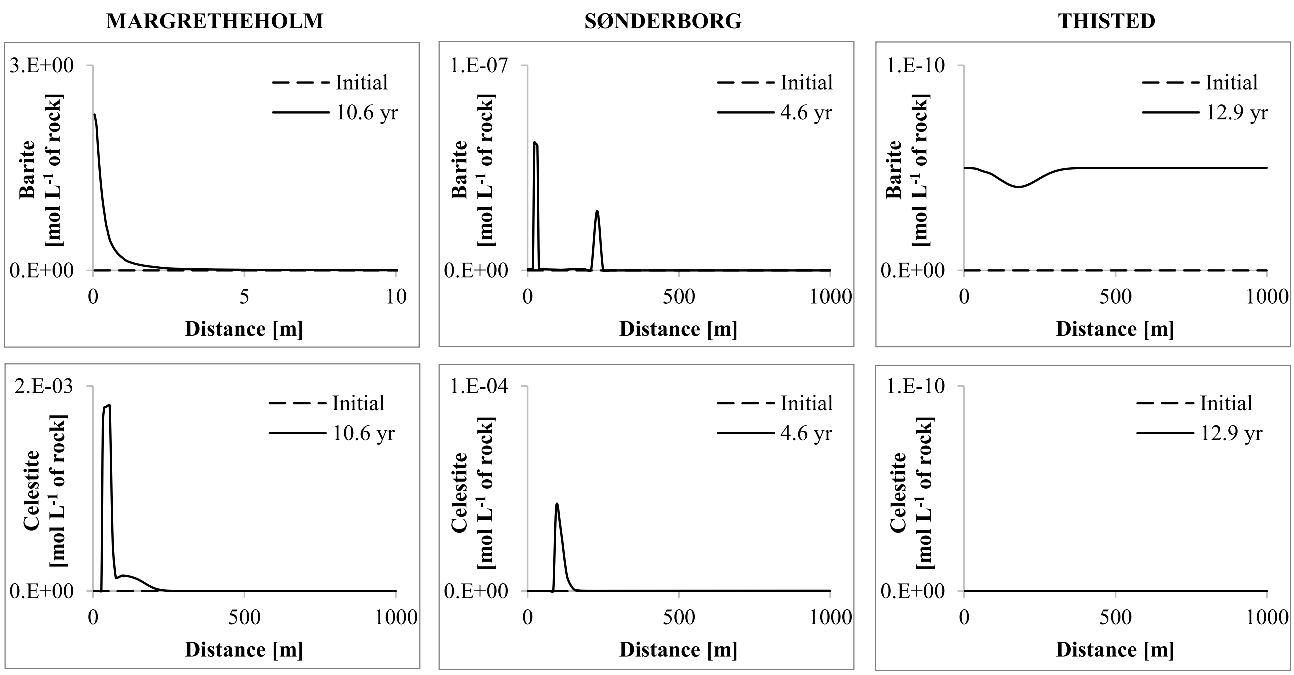

Fig. 6. Amounts of barite and celestite calculated in 2D axisymmetric simulations after 10.6, 4.6 and 12.9 years for the Margretheholm, Sønderborg and Thisted geothermal plant, respectively.

3.2. Mineral precipitation and dissolution in the reservoir – 2D models

3.2.1. Sulphates – barite and celestite

2D axisymmetric simulations indicated barite precipitation (Fig. 6). This mainly affected the near field of the injection wells. Barite is one of the most common scaling minerals that precipitates over a wide range of temperatures, pressures and hydrogeochemical conditions (Bosbach, 2002; Zhen-Wu et al., 2016; Lu et al., 2020). The results of the speciation calculations suggested that the highest risk of barite precipitation was in the Margretheholm geothermal plant (Fig. 3), in both, the geothermal loop after the heat exchanger and in the reservoir. The highest barite amount of up to 2.3 mol L^{-1} of rock was predicted in Margretheholm within 5 m from the injection well (Fig. 6). Thus, the barite precipitation in Margretheholm was likely to take place immediately upon the injection of the cooled brine into the reservoir, assuming that the chemistry of the cooled brine at the bottom of the injection well was similar to the chemistry of the water sampled prior to the injection at the top of the well. The precipitation of insignificant amounts of barite was also predicted in Sønderborg and Thisted (Figs. 3 and 6). 2D axisymmetric simulations indicated also celestite precipitation in the near field of the injection wells in Margretheholm and Sønderborg in an amount of up to 1.8×10^{-3} mol L^{-1} of rock in Margretheholm (Fig. 6). Celestite was expected to precipitate at 50–100 m from the injection well.

Bhandari et al. (2016) found that at a given temperature barite precipitation rates increase with an increasing pressure. This indicates that barite precipitation was likely to take place in the Margretheholm geothermal reservoir. If the precipitation of barite took place in the reservoir, the larger amount of barite particles was not detected in the above ground facilities. The modelling results are confirmed by the observations in the Margretheholm geothermal plant, where small amounts of barite and celestite were found in the geothermal loop (Laier, pers. com.) and injectivity problems were experienced after one year of operation. To maintain the flow rate, the injection pressure in the Margretheholm geothermal plant was increased by a factor of 7. The likely explanation for the injectivity problems in the Margretheholm reservoir is barite precipitation in the near field of the injection well, as indicated by geochemical modelling. Barite precipitation in Margretheholm takes place despite of the higher flux rates compared to the geothermal plants in Sønderborg and Thisted.

Geochemical modelling of the water in the Sønderborg and Thisted geothermal reservoirs suggested precipitation of insignificant barite amounts (Fig. 6), as the decrease in the brine temperature after the heat extraction was small (Table 2). This is in line with no injectivity problems experienced in the Thisted geothermal plant during 30 years of a plant operation. The injectivity problems observed in Sønderborg cannot be explained by barite precipitation and the modelling results suggest that other causes than chemical clogging exist.

Barite is one of the common scales in oil production (Oliveira et al., 2019) and in geothermal plant installations (Banks et al., 2014; Bozau et al., 2015), and celestite is often a co-occurring solid phase (Banks et al., 2014; Nitschke et al., 2014). Ba and Sr in the brines probably originate from diagenetic alteration of K-feldspar, thereby liberating Ba, which substitutes for K, and anhydrite, in which small amounts of Ba and Sr may replace Ca (Deer et al., 1985). The Bunter Sandstone Formation is characterized by both rare anhydrite cement and common K-feldspar, and hence *in situ* potential internal sources for Ba and Sr. Barite formation is essentially promoted by cooling of the fluid after heat extraction due to the decrease in the solubility of the salt with the decreasing temperature (Bozau et al., 2015; Cazenave et al., 2020).

The surface area of pure barite used in the laboratory experiments to determine the mineral dissolution and precipitation rates is from 10^{-3} to 0.5 $m^2\ g^{-1}$ (Bosbach, 2002; Banks et al., 2014; Zhen-Wu et al., 2016). However, the mineral precipitation takes place mostly only on the few edge sites (Zhen-Wu et al., 2016) and the reactive surface area is often a couple of orders of magnitude smaller than the total surface area (Bosbach, 2002; Zhu, 2003; Banks et al., 2014). Furthermore, the reactive surface area of barite increases with an increasing supersaturation and at the room temperature is equal to the total surface area at the SI > 380 with respect for barite (Bosbach, 2002). In the investigated geothermal plants the SI of cooled brine with respect to barite ranged from 0.5 at Sønderborg to 1.2 at Margretheholm. Therefore, a reactive surface area of $2 \times 10^{-5}\ m^2\ g^{-1}$ considered in this study was a realistic value.

The specific surface area available for the barite precipitation used in the 2D axisymmetric simulations was adjusted to the porosity changes predicted in the Margretheholm reservoir. A sensitivity analysis has been made by varying the specific surface area from 10^{-5} to $5 \times 10^{-5}\ m^2\ g^{-1}$. The amount of the precipitated barite and thereby the porosity changes were very sensitive to the surface area. The reactive surface area of $5 \times 10^{-5}\ m^2\ g^{-1}$ clearly led to an overestimation of the precipitated amount of barite and after 10.6 years of the water-rock interactions, the mineral formation led to a massive clogging of the porosity in the near field of the injection well (Fig. 7). The result disagreed with the flow rates recorded during the operating period. The reactive surface areas of 2×10^{-5} and $10^{-5}\ m^2\ g^{-1}$ appeared to be more realistic (Fig. 7) and were compatible with the observed flow rates. Nonetheless, the formation of barite was almost totally inhibited considering the reactive surface area of $10^{-5}\ m^2\ g^{-1}$, while the saturation index for barite was > 1. At this saturation level the precipitation of barite takes place over a wide range of temperatures, pressures and hydrogeochemical conditions (Zhen-Wu et al., 2016). Therefore, a reactive surface area of $2 \times 10^{-5}\ m^2\ g^{-1}$ was considered in this study.

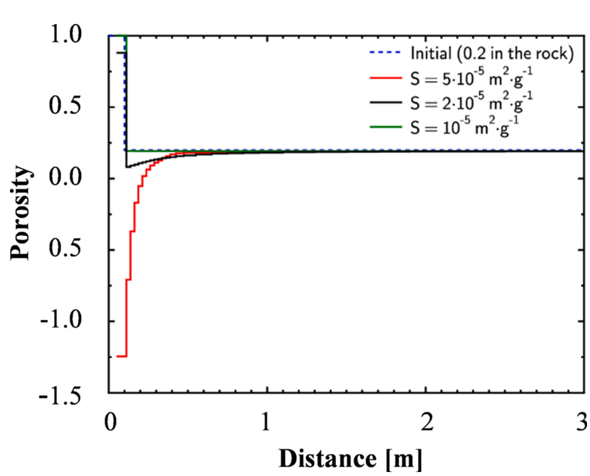

Fig. 7. Sensitivity study of the reactive surface area of barite in 2D axisymmetric simulation for the Margretheholm and its effect on the reservoir porosity changes after 10.6 years of the geothermal plant operation.

3.2.2. *Carbonates – calcite and dolomite*

Results of a 2D axisymmetric MARTHE-PHREEQC model indicated a dissolution of dolomite and precipitation of calcite in the Margretheholm reservoir and the dissolution of small amounts of calcite and dolomite in the Sønderborg and Thisted reservoirs as the cooling front progressed (Fig. 8). The conversion between dolomite and ankerite, which is approximately equivalent to the conversion between dolomite and calcite, has been observed in low temperature batch experiments of CO_2-water-basalt interaction (Gysi and Stefánsson, 2012) and iron-bearing dolomite dissolution (Debure et al., 2017). Conversions between calcite and dolomite were especially important in the Margretheholm reservoir, where calcite and dolomite were 6.4% of the mass fraction (Table 1). The initial amount of dolomite in the Sønderborg reservoir and calcite in the Thisted reservoir were 0.02% and 0.01% of the mass fraction, respectively (Table 1). Thus, calcite and dolomite dissolution in these reservoirs would not have a significant influence on the reservoir structure in the near field of the injection wells.

The results of speciation calculations indicated the saturation of the cooled brine in Margretheholm with calcite and dolomite (Fig. 3). Calcite precipitates are found in the oil pipelines (Oliveira et al., 2019) and in the geothermal plants (Demir et al., 2014; Wanner et al., 2017) when a degassing of fluid takes place. Thus, a similar process could be expected in the geothermal plants. However, as the geothermal loops were sealed for the gas loss, the magnitude of the process was probably overestimated by the model, as carbonate minerals have been processed at the local equilibrium, excluding the kinetics. Furthermore, calcite or dolomite scaling was not observed along the wells or at the well heads.

3.3. *Precipitation and dissolution of Al-bearing minerals in the reservoir – 1D models*

The results of the 1D reactive transport modelling indicated the dissolution and precipitation, although of minor importance, of Al-bearing minerals (K-feldspar, kaolinite, illite and chlorite) upon injection of the cooled formation water into the reservoirs and progression of the cooled front. These results, however, must be interpreted with caution, as saturation indices and activity coefficients calculated using *phreeqc.dat* differ slightly from the results of calculations based on *pitzer.dat* (Figs. 4 and 5).

K-feldspar altered to kaolinite and/or chlorite in the geothermal plants. The process took place mainly in the cooled down parts of the reservoir in Margretheholm. In the near field (up to 5 m distance) of the injection wells in the three geothermal plants chlorite and K-feldspar dissolved whereas kaolinite precipitated. Kaolinite is a common precipitate during hydrothermal changes in sedimentary geothermal reservoirs at temperatures < 115 °C (Giorgetti et al., 2000), however, its precipitation kinetics are slow (Devidal et al., 1997). Therefore, the amount of precipitated kaolinite might have been overestimated by a simulation that used an equilibrium state. Additionally, the order of transformations was probably overestimated, as the chlorite dissolution rate at pH 5–7 and temperatures up to 80 °C is low and of the order 10^{-12} mol $m^{-2}\ s^{-1}$ (Smith and Carroll, 2016). Ions for the formation of kaolinite and chlorite are derived from K-feldspar and muscovite dissolution (Giorgetti et al., 2000; Xiao et al., 2018), as modelled for the Danish geothermal reservoirs.

Illite, was dissolved at low temperatures in Margretheholm and Sønderborg, although in small quantities, as it constituted < 1% of the reservoir composition (Table 1). Kaolinite is transformed into illite at approximately 200 °C (Giorgetti et al., 2000). The temperatures in the geothermal reservoirs at the depth of the injection well did not exceed 74 °C (Fig. 1) and illite dissolution was possible. The remaining Al-bearing minerals (albite, muscovite) were neither precipitated nor dissolved in the reservoirs. Precipitation or dissolution of amorphous

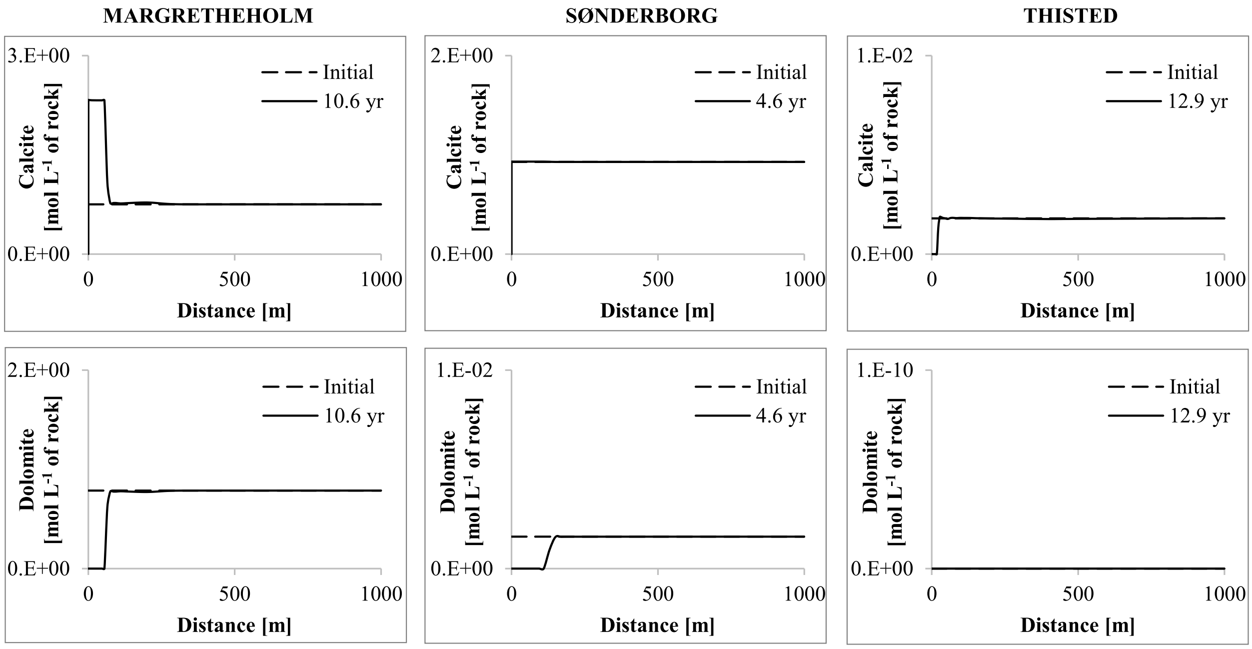

Fig. 8. Amounts of calcite and dolomite calculated in 2D axisymmetric simulations after 10.6, 4.6 and 12.9 years for the Margretheholm, Sønderborg and Thisted geothermal plant, respectively.

silica and quartz in the time periods up to 12.9 years in the Danish geothermal reservoirs was unlikely according to the model.

The influence of the conversion between Al-bearing minerals on the performance of the geothermal plants could be neglected, as it probably did not significantly change the reservoir porosity. It has also been shown that dissolution of K-feldspar and precipitation of chlorite, illite and kaolinite improves the reservoir porosity, if the concentration of these phases is smaller than 12, 4 and 3%, respectively (Xiao et al., 2018). The concentration of the clay minerals in the geothermal reservoirs (Table 1) was below these threshold values. However, if substantial amounts of chlorite, illite and kaolinite would precipitate, the permeability might be affected (Xiao et al., 2018) and brine migration may become a problem.

3.4. Porosity changes in the reservoir

The porosity profile simulated in MARTHE-PHREEQC for Margretheholm, Sønderborg and Thisted geothermal reservoirs indicated that the porosity of the reservoir might have been reduced near the injection well in the Margretheholm geothermal plant, while no changes were expected in the Sønderborg and Thisted geothermal plants (Fig. 9). The reduction of the reservoir porosity and permeability has been observed due to e.g. barite precipitation (Griffiths et al., 2016) or quartz precipitation at the greater depths (White and Mroczek, 1998). The reduced porosity decreases the reservoir injectivity and an increase of the injection pressure is required to maintain the constant flow rate at the injection well, as has been observed during the operation of the Margretheholm geothermal plant (Laier, pers. com.). The flow rate in Margretheholm decreased from 241 $m^3 h^{-1}$ to approximately 120 $m^3 h^{-1}$ despite an increase in the injection pressure.

Particularly precipitation of barite near the injection well in Margretheholm may be partly responsible for the reduction of the reservoir porosity, and to a lesser degree the precipitation of celestite (Fig. 6). The porosity of barite, celestite and calcite scales collected from the oil pipes is up to 13% (Oliveira et al., 2019). This is significantly lower than the porosity in the geothermal reservoirs. Furthermore, the injectivity in the Margretheholm geothermal plant increased after acidification of the well, although the improvement was temporal (Laier, pers. com.). The possible reason was the increased rate of barite dissolution at the decreased pH, as barite precipitation and dissolution rates are pH dependant (Zhen-Wu et al., 2016). Under the regular operation of the geothermal plant pH increased and barite might have precipitated. Precipitation of barite in the Margretheholm reservoir cannot be excluded as one of the reasons for the injectivity problems. Porosity changes modelled with MARTHE-PHREEQC are a quantitative estimate and modelled precipitation does not change a number and distribution of pore throats available for water flow. Thus, the flow patterns are not affected by porosity changes, although a decrease in pore water velocities takes place.

Modelling results rule out chemical clogging as the reason for the

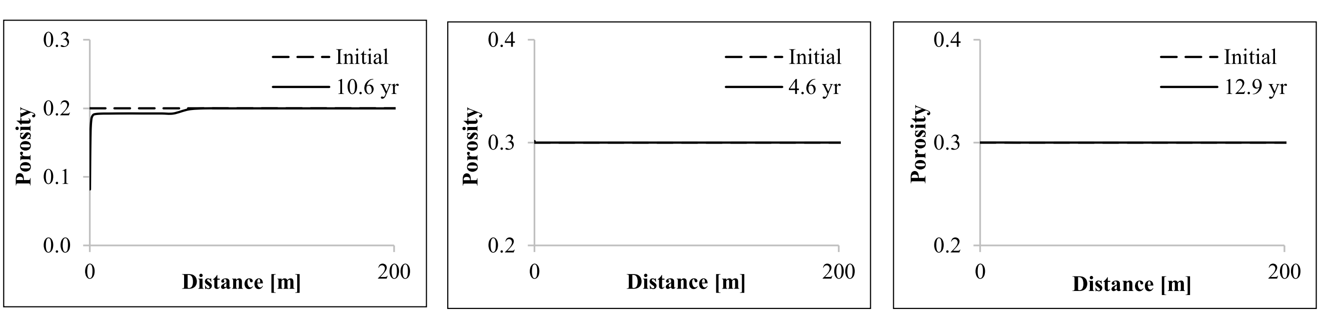

Fig. 9. Porosity profile calculated after 10.6 years of production in the Margretheholm geothermal reservoir, after 4.6 years of production in the Sønderborg geothermal reservoir and after 12.9 years of production in the Thisted geothermal reservoir.

injectivity problems observed in the Sønderborg geothermal plant, where at the constant injection pressure the flow rate decreased from approximately 170 $m^3 h^{-1}$ to 70 $m^3 h^{-1}$. Physical and biological clogging have been identified as common problems at geothermal plants (Song et al., 2020) and may also take place in Sønderborg; however, further investigations are needed to evaluate if this is likely or if the injection problems are related to technical issues.

Transformations between calcite and dolomite (Fig. 8) and Al-bearing minerals did not significantly increase the volume of the minerals in the geothermal reservoirs, and therefore contributed to the porosity changes to a negligible degree. Transformations between calcite and dolomite do not have an important influence on the reservoir porosity and performance of the geothermal plants as also seen for oil reservoirs (Rodriguez-Morillas et al., 2013). Replacement of K-feldspar with chlorite, illite and kaolinite may increase the reservoir porosity (Xiao et al., 2018), but probably reduce the permeability.

3.5. Barite nucleation in the injection well

Modelling of the injection of cooled formation water into the reservoirs indicated that barite may precipitate near the injection wells, particularly in the Margretheholm geothermal plant. Therefore, the possibility of barite nucleation in the injection wells was investigated, as the mineral is often found in the oil pipes (Oliveira et al., 2019) and in geothermal heat exchangers (Cazenave et al., 2020).

Barite nucleation was possible in the injection well in Margretheholm geothermal plant and appeared to be unlikely in the injection wells in Sønderborg and Thisted geothermal plants (Fig. 10). The barite nucleation rate depends on several parameters such as the formation water composition, temperature, pressure, barite saturation index, ionic strength of the solution and the surface area on which the mineral grows (Lu et al., 2020; in prep. Dideriksen et al.). The modelling indicated that even though the temperature of the cooled brines favoured barite formation, the nucleation could be expected only for SI > 1. Zhen-Wu et al. (2016) found that the equilibrium state for barite is at the saturation index of 1 for a wide range of physical parameters and hydrogeochemical properties. The results of flowing tube experiments by Lu et al. (2020) also indicated the significance of supersaturation for deposition kinetics of barite. SI for barite in the Margretheholm geothermal plant was 1.2 at 20 °C, while in Sønderborg and Thisted it equalled 0.5 (16 °C) and 0.8 (16 °C), respectively (Fig. 3). Although barite nucleation in the Margretheholm injection well was likely, the SI of the cooled brine for barite was close to the equilibrium state, and according to the modelling results only a small amount of barite formed in the uppermost part of the well (Fig. 10), as the barite deposition rate decreases along the tubing (Lu et al., 2020). Including induction time in

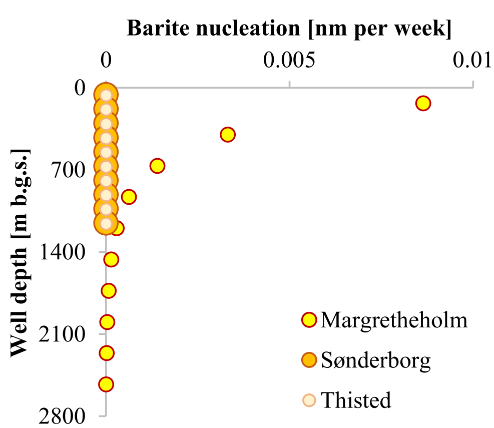

Fig. 10. Barite nucleation at the injection wells. The x-axis indicates the expected thickness of a barite layer precipitated within one week of the geothermal plant operation.

the calculations, would further decrease the predicted amount of barite (He et al., 1995).

The calculated barite quantities nucleated in the Margretheholm geothermal plant were small. The simulated weekly maximal growth of barite crystals equalled 8.64×10^{-11} m (Fig. 10). This gave an annual growth of 2×10^{-10} m, considering only the operation months. Cazenave et al. (2020) simulated a theoretical annual barite growth in the heat exchanger of 3×10^{-6} m. Turbulence in the flow caused by obstacles is considered as one of the most important parameters in barite scale formation (Sutherland et al., 2013). A small amount of barite and celestite scaling in the pipes in the Margretheholm geothermal plant was found near taps (Laier, pers. com.), which fits with the modelled low volumes of barite precipitated and the influence of turbulence. The modelling results also indicated that the nucleation of barite in Margretheholm geothermal plant was a fast process that might have taken place immediately after cooling of the formation water in the heat exchanger. However, the amount of barite would have no impact on the injection well. Barite scaling in the Margretheholm geothermal loop has previously been ruled out as a significant process (Laier, 2002), and it has been suggested that the injection problems in Margretheholm may be caused by the precipitation of metallic lead due to galvanic corrosion (Laier, 2015a; T. 2015b; 2015c). Furthermore, (in prep. Dideriksen et al.) developed the barite nucleation model for the oil wells. Thus, there is an uncertainty in the nucleation rates, as the nucleation model was not tested before in the geothermal plants.

4. Conclusions

Barite precipitation in the reservoirs may be a major challenge in the functioning of some of the Danish geothermal plants and the risk may need to be considered and mitigated, as shown by the modelling results. Precipitation and dissolution of carbonates, Al-bearing and clay minerals are considered to be of minor importance in the geothermal plants.

Precipitation of barite, a common scale in geothermal plants (e.g. Banks et al., 2014; Bozau et al., 2015; Cazenave et al., 2020), may be partly responsible for a reduction of the porosity in the reservoir and thus the injection problems in the Margretheholm geothermal plant. Due to the fast kinetics of the barite formation, nucleation of the mineral can be expected in the injection well, although the amount of barite formed is small. Injectivity problems in the Sønderborg geothermal plant could not be explained by chemical clogging due to scaling and are rather an effect of technical problems or physical or biochemical clogging.

Chemical clogging and porosity reduction are not a risk in Thisted, the oldest geothermal plant in Denmark that has been running without problems since 1984. It is an advantage from an energy, climate and economical perspective.

The results of the hydrogeochemical modelling emphasise the need for a thorough understanding of the reservoir mineralogy and the chemical composition of the geothermal brine. Such detailed data can be utilized for geochemical modelling that investigates if problems may arise over time in the geothermal loop. The modelling results may also suggest efforts that can mitigate potential problems. In this way a sustainable exploitation of geothermal energy can be ensured.

CRediT authorship contribution statement

Jolanta Kazmierczak: Conceptualization, Methodology, Formal analysis, Data curation, Writing – original draft, Writing – review & editing, Visualization, Supervision. **Nicolas Marty:** Conceptualization, Methodology, Formal analysis, Writing – original draft, Writing – review & editing. **Rikke Weibel:** Writing – original draft, Writing – review & editing. **Lars Henrik Nielsen:** Data curation, Writing – review & editing, Funding acquisition. **Hanne Dahl Holmslykke:** Conceptualization, Investigation, Writing – original draft, Writing – review & editing, Supervision.

Declaration of Competing Interest

The authors declare that they have no known competing financial interests or personal relationships that could have appeared to influence the work reported in this paper.

Data availability

Data will be made available on request.

Acknowledgment

The research was sponsored by an Innovation Fund grant #6154-0001.

References

Andritsos, N., Karabellas, A.J., 1991. Sulfide scale formations and control: the case of lead sulfide. Geothermics 20, 343–353. https://doi.org/10.1016/0375-6505(91)90025-Q.

Andritsos, N., Karabelas, A.J., Koutsoukos, P., 2002. Scale formation in geothermal plants. Int. Summ. School Direct Appl. Geotherm. Energy 179–189.

Appelo, C.A.J., Postma, D., 2005. Geochemistry, Groundwater and Pollution, 2nd ed. A. A. Balkema Publishers, Leiden, The Netherlands, p. 649.

Balling, N., Major, M., Fuchs, S., Mathiesen, A., Nielsen, C.M., Hansen, T.M., Kristensen, L., Förster, A., 2019. Geothermal reservoirs in the Danish area: temperatures, resources and models for long-term energy extraction. Innovation Fund Denmark: project 6154-00011B Final report in WP4. Aarhus University, Aarhus, Denmark, p. 70.

Banks, J., Regenspurg, S., Milsch, H., 2014. Experimental method for determining mixed-phase precipitation kinetics from synthetic geothermal brine. Appl. Geochem. 47, 74–84. https://doi.org/10.1016/j.apgeochem.2014.05.016.

Bhandari, N., Kan, A.T., Zhang, F., Dai, Z., Yan, F., Ruan, G., Zhang, Z., Liu, Y., van Eldik, R., Tomson, M.B., 2016. Mineral precipitation kinetics: assessing the effect of hydrostatic pressure and its implication on the nucleation mechanism. Cryst. Growth Des. 16, 4846–4854. https://doi.org/10.1021/acs.cgd.6b00126.

Bosbach, D., 2002. Linking molecular-scale barite precipitation mechanisms with macroscopic crystal growth rates. Water Rock Interact. Ore Depos. Environ. Geochem. 7, 97–110.

Bozau, E., Häußler, S., van Berk, W., 2015. Hydrogeochemical modelling of corrosion effects and barite scaling in deep geothermal wells of the North German Basin using PHREEQC and PHAST. Geothermics 53, 540–547. https://doi.org/10.1016/j.geothermics.2014.10.002.

Carroll, S., Mroczek, E., Alai, M., Ebert, M., 1998. Amorphous silica precipitation (60 to 120C): comparison of laboratory and field rates. Geochim. Cosmochim. Acta 62, 1379–1396. https://doi.org/10.1016/S0016-7037(98)00052-0.

Cazenave, F., Bernada, P., Couture, F., Serin, J.P., 2020. Modelling of solid formation by heterogeneous reactions through a multicomponent transport model of diluted ionic species: simulation of barite fouling in a geothermal heat exchanger. Can. J. Chem. Eng. 98, 979–997. https://doi.org/10.1002/cjce.23672.

Clemmensen, L.B., 1985. Desert sand plain and sabkha deposits from the Bunter Sandstone Formation (L. Triassic) at the northern margin of the German Basin. Geol. Rundsch. 74, 519–536.

Debure, M., Andreazza, P., Canizarès, A., Grangeon, S., Lerouge, C., Mack, P., Madé, B., Simon, P., Veron, E., Warmont, F., Vayer, M., 2017. Study of iron-bearing dolomite dissolution at various temperatures: evidence for the formation of secondary nanocrystalline iron-rich phases on the dolomite surface. ACS Earth Space Chem. 1, 442–454. https://doi.org/10.1021/acsearthspacechem.7b00073.

Deer, W.A., Howie, R.A., Zussman, J., 1985. An Introduction of the Rock Forming Minerals. Longman group Limited, p. 528.

Demir, M.M., Baba, A., Atilla, V., Inanli, M., 2014. Types of the scaling in hyper saline geothermal system in northwest Turkey. Geothermics 50, 1–9. https://doi.org/10.1016/j.geothermics.2013.08.003.

Devidal, J.L., Schott, J., Danurand, J.L., 1997. An experimental study of kaolinite dissolution and precipitation kinetics as a function of chemical affinity and solution composition at 150°C, 40 bars, and pH 2, 6.8, and 7.8. Geochim. Cosmochim. Acta 61 (24), 5165–5186. https://doi.org/10.1016/S0016-7037(97)00352-9.

Fritz, B., Noguera, C., 2009. Mineral precipitation kinetics. Rev. Miner. Geochem. 70, 371–410. https://doi.org/10.1021/acs.cgd.6b00126.

Fuchs, S., Balling, N., Mathiesen, A., 2020. Deep basin temperature and heat-flow field in Denmark – New insights from borehole analysis and 3D geothermal modelling. Geothermics 83, 1–18. https://doi.org/10.1016/j.geothermics.2019.101722.

Ganor, J., Huston, T.J., Walter, L.M., 2005. Quartz precipitation kinetics at 180̊C in NaCl solutions – Implications for the usability of the principle of detailed balancing. Geochim. Cosmochim. Acta 69, 2043–2056. https://doi.org/10.1016/j.gca.2004.09.026.

Giorgetti, G., Mata, M.P., Peacor, R., 2000. TEM study of the mechanism of transformation of detrital kaolinite and muscovite to illite/smectite in sediments of the salton sea geothermal field. Eur. J. Miner. 12, 923–934. https://doi.org/10.1127/0935-1221/2000/0012-0923.

Griffiths, L., Heap, M.J., Wang, F., Daval, D., Gilg, H.A., Baud, P., Schmittbuhl, J., Genter, A., 2016. Geothermal implications for fracture-filling hydrothermal precipitation. Geothermics 64, 235–245. https://doi.org/10.1016/j.geothermics.2016.06.006.

Gysi, A.P., Stefánsson, A., 2012. CO_2-water–basalt interaction. Low temperature experiments and implications for CO_2 sequestration into basalts. Geochim. Cosmochim. Acta 81, 129–152. https://doi.org/10.1016/j.gca.2011.12.012.

He, S., Oddo, J.E., Tomson, M., 1995. The nucleation kinetics of barium sulfate in NaCl solutions up to 6m and 90°C. J. Colloid Interface Sci. 174, 319–326. https://doi.org/10.1006/jcis.1995.1397.

Hjuler, M.L., Kristensen, K., Laier, T., Boldreel, L.O., Olivarius, M., Nielsen, L.H., Mathiesen, A., Nielsen, C.M., 2019. A multidisciplinary study of the geothermal potential in the Tønder area, Southern Jutland, Denmark. Geothermics 78, 211–223. https://doi.org/10.1016/j.geothermics.2018.12.001.

Holmslykke, H.D., Schovsbo, N.H., Kristensen, L., Weibel, R., Nielsen, L.H., 2019. Characterizing brines in deep Mesozoic sandstone reservoirs, Denmark. GEUS Bull. 43 https://doi.org/10.34194/GEUSB-201943-01-04.

Hsu, P.H., 2006. Nucleation, polymerization and precipitation of FeOOH. J. Soil Sci. 23, 409–419. https://doi.org/10.1111/j.1365-2389.1972.tb01671.x.

Konikow, L.F., 2010. The secret to successful solute-transport modeling. Groundwater 49 (2), 144–159. https://doi.org/10.1111/j.1745-6584.2010.00764.x.

Kristensen, L., Hjuler, M.L., Frykman, P., Olivarius, M., Weibel, R., Nielsen, L.H., Mathiesen, A., 2016. Pre-drilling assessments of average porosity and permeability in geothermal reservoirs of the Danish area. Geotherm. Energy 4 (6), 1–27. https://doi.org/10.1186/s40517-016-0048-6.

Laier, T., 2002. Vurdering af udfældningsrisici ved geotermisk produktion fra Margretheholm. MAH-1A. Beregning af mætningsindeks for mineraler i saltvand fra Danmarks dybere undergrund. GEUS Rapport, 2002/95.

Laier, T., 2015a. Blypartikler i Posefiltre På GDA Skyldes Muligvis Midlertidige Blyudfældninger i Anlæg. GEUS Letter, p. 10.

Laier, T., 2015b. Bly i Belægninger Og Posefiltre På GDA. GEUS Letter, p. 8.

Laier, T., 2015c. Lead in formation water causes problems in geothermal exploitation at Margretheholm. GEUS Letter 21.

Laier, T., 2015d. Membranfilterprøver, viser zinksulfid og blysulfid i Sønderborg geotermiske anlæg. GEUS Notat 20, 17 april 2015.

Laier, T., 2016. Mikrobiel sulfiddannelse i Sønderborgs geotermiske anlæg. GEUS Notat 25, 10 februar 2016.

Lasaga, A.C., 1981. Transition state theory. Rev. Miner. Geochem. 8, 135–168.

Lu, A.Y.T., Harouaka, K., Paudyl, S., Ko, S., Dai, C., Gao, S., Deng, G., Zhao, Y., Wang, X., Mateen, S., Kan, A.T., Tomson, M., 2020. Kinetics of barium sulfate deposition and crystallization process in the flowing tube. Ind. Eng. Chem. Res. 59, 7299–7309. https://doi.org/10.1021/acs.iecr.0c00112.

Ng, D.Q., Chen, C.Y., Lin, Y.P., 2018. A new scenario of lead contamination in potable water distribution systems: galvanic corrosion between lead and stainless steel. Sci. Total Environ. 637, 1423–1431. https://doi.org/10.1016/j.scitotenv.2018.05.114.

Nielsen, L.H., 2003. Late triassic-jurassic development of the Danish basin and the fennoscandian border zone, southern scandinavia. In The Jurassic of Denmark and Greenland; Ineson, J. R., Surlyk, F., Eds GEUS Bull. 1, 459–526. https://doi.org/10.34194/geusb.v1.4681.

Nielsen, M.T., Olivarius, M., Weibel, R., Mathiesen, A., Tremosa, J., Bonnell, L., Nielsen, J.H., 2019. Geothermal Reservoir Quality Prediction from Diagenesis modelling. European Geothermal Congress 2019. Den Haag, The Netherlands, pp. 11–14.

Nitschke, F., Scheiber, J., Kramar, U., Neumann, T., 2014. Formation of alternating layered Ba-Sr-sulfate and Pb-sulfide scaling in the geothermal plant of Soultz-sous-Forêts. N. Jb. Miner. Abh. (191/2), 145–156. https://doi.org/10.1127/0077-7757/2014/0253.

Olivarius, M., Weibel, R., Hjuler, M.L., Kristensen, L., Mathiesen, A., Nielsen, L.H., Kjøller, C., 2018. Diagenetic effects on porosity-permeability relationships in red beds of the Lower Triassic Bunter Sandstone Formation in the North German Basin. Sediment. Geol. 321, 139–153. https://doi.org/10.1016/j.sedgeo.2015.03.003.

Olivarius, M., Nielsen, L.H., 2016. Triassic paleogeography of the greater eastern Norwegian-Danish Basin: constraints from provenance analysis of the Skagerrak Formation. Mar. Pet. Geol. 69, 168–182. https://doi.org/10.1016/j.marpetgeo.2015.10.008.

Olivarius, M., Laier, T., Knudsen, C., Malkki, S.H., Thomsen, T.B., Serre, S.H., Kristensen, L., Willumsen, M.E., Nielsen, L.H., 2018. Source and occurrence of radionuclides in geothermal water. With focus on the Margretheholm geothermal plant. GEUS Rep. 77, 2018/41.

Oliveira, D.F., Santos, R.S., Machado, A.S., Silva, A.S.S., Anjos, M.J., Lopes, R.T., 2019. Characterization of scale deposition in oil pipelines through X-Ray Microfluorescence and X-Ray microtomography. Appl. Radiat. Isot. 151, 247–255. https://doi.org/10.1016/j.apradiso.2019.06.019.

Olsen, H., 1987. Ancient ephemeral stream deposits: a local terminal fan model from the bunter sandstone formation (L. Triassic) in the Tønder-3, -4 and -5 wells, Denmark. In: Frostick, L., Reid, I. (Eds.), Desert Sediments: Ancient and Modern Geol. Soc. Spec. Publ 35, 69–86.

Palandri, J., Kharaka, Y., 2004. A compilation of rate parameters of water-mineral interaction kinetics for application to geochemical modeling. USGS Rapport 1068, 71.

Parkhurst, D.L., Appelo, C., 2013. Description of input and examples for PHREEQC version 3—a 723 computer program for speciation, batch-reaction, one-dimensional transport, and inverse 724 geochemical calculations. USGS techniques and methods. Book 6, 497.

Rimstidt, J.D., Barnes, H.L., 1980. The kinetics of silica-water reactions. Geochim. Cosmochim. Acta 44, 1683–1699. https://doi.org/10.1016/0016-7037(80)90220-3.

Rodriguez-Morillas, N., Playa, E., Travé, A., Martin-Martin, J., 2013. Diagenetic processes in a partially dolomitized carbonate reservoir: casablanca oil field, Mediterranean Sea, offshore Spain. Geol. Acta 11, 195–214. https://doi.org/10.1344/105.000001839.
Smith, M.M., Carroll, S.A., 2016. Chlorite dissolution kinetics at pH 3-10 and temperature to 275°C. Chem. Geol. 421, 55–64. https://doi.org/10.1016/j.chemgeo.2015.11.022.
Song, W., Liu, X., Zheng, T., Yang, J., 2020. A review of recharge and clogging in sandstone aquifer. Geothermics 87, 1–12. https://doi.org/10.1016/j.geothermics.2020.101857.
Sutherland, L., Johnston, C., Taylor, W., 2013. The influence of turbulence (or hydrodynamic effects) on barium sulphate scaling formation and inhibitor performance. In: Proceedings of the SPE International Symposium on Oilfield Chemistry Location. The Woodlands, TX, USA. https://doi.org/10.2118/164070-MS.
Thiéry, D., 2015. Modélisation 3D Du Transport Réactif avec Le Code De Calcul MARTHE v7.5 Couplé Aux Modules Géochimiques De PHREEQC. Orléans, France, p. 164. BRGM/RP-65010-FR, R.
Tonkul, S., Baba, A., Demir, M.M., Regenspurg, S., 2021. Characterization of Sb scaling and fluids in saline geothermal power plants: a case study of Germenick Region (Büyük Menderes Graben, Turkey). Geothermics 96, 1–28. https://doi.org/10.1016/j.geothermics.2021.102227.
Trémosa, J., Castillo, C., Vong, C.Q., Kervévan, C., Lassin, A., Audigane, P., 2014. Long-term assessment of geochemical reactivity of CO_2 storage in highly saline aquifers: application to Ketzin, In Salah and Snøhvit storage sites. Int. J. Greenh. Gas Control 20, 2–26. https://doi.org/10.1016/j.ijggc.2013.10.022.
Vinsome, P., Westerveld, J., 1980. A simple method for predicting cap and base rock heat losses in thermal reservoir simulators. J. Can. Pet. Technol. 19 (03) https://doi.org/10.2118/80-03-04, 10.2118/80-03-04.
Vosgerau, H., Mathiesen, A., Kristensen, L., Andersen, M.S., Hjuler, M.L., Laier, T., 2015a. Det geotermiske screeningsprojekt. Hillerød-lokaliteten. GEUS Rapp 15, 33, 2015/.
Vosgerau, H., Mathiesen, A., Kristensen, L., Andersen, M.S., Hjuler, M.L., Laier, T., 2015b. Det geotermiske screeningsprojekt. Sønderborg-lokaliteten. GEUS Rapport 30, 2015/33.
Wanner, C., Eichinger, F., Jahrfeld, T., Diamond, L.W., 2017. Causes of abundant calcite scaling in geothermal wells in the Bavarian Molasse Basin, Southern Germany. Geothermics 70, 324–338. https://doi.org/10.1016/j.geothermics.2017.05.001.
Weibel, R., Friis, H., 2004. Opaque minerals as keys for distinguishing oxidising and reducing diagenetic conditions in the Lower Triassic Bunter Sandstone, North German Basin. Sediment. Geol. 169, 129–149.
Weibel, R., Olivarius, M., Friis, H., Kristensen, L., Hjuler, M.L., Kjøller, C., Pedersen, P.K., Boyce, A., Mathiesen, A., Nielsen, L.H., 2017a. The influence of climate on early and burial diagenesis in Triassic and Jurassic sandstones from the Norwegian–Danish Basin. Depos. Rec. 3 (1), 60–91, 0.1002/dep2.27.
Weibel, R., Olivarius, M., Kristensen, L., Friis, H., Hjuler, M.L., Kjøller, C., Mathiesen, A., Nielsen, L.H., 2017b. Predicting permeability of low enthalpy geothermal reservoirs: a case study from the upper triassic-lower Jurassic Gassum formation, Norwegian-Danish basin. Geothermics 65, 135–157. https://doi.org/10.1016/j.geothermics.2016.09.003.
Weibel, R., Olivarius, M., Vosgerau, H., Mathiesen, A., Kristensen, L., Nielsen, C.M., Nielsen, L.H., 2020. Overview of potential geothermal reservoirs in Denmark. Neth. J. Geosci. 99, 1–14. https://doi.org/10.1017/njg.2020.5 e3.
White, S.P., Mroczek, E.K., 1998. Permeability changes during the evolution of a geothermal field due to the dissolution and precipitation of quartz. Transp. Porous Med. 33, 81–101. https://doi.org/10.1155/2018/6957306.
Xiao, M., Yuan, X., Cheng, D., Wu, S., Cao, Z., Tang, Y., Xie, Z., 2018. Feldspar dissolution and its influence on reservoirs: a case study of the Lower Triassic Baikouquan Formation in the Northwest Margin of the Junggar Basin, China. Geofluids 1–19. https://doi.org/10.1155/2018/6536419.
Zhen-Wu, B.Y., Dideriksen, K., Olsson, J., Raahauge, P.J., Stipp, S.L.S., Oelkers, E.H., 2016. Experimental determination of barite dissolution and precipitation rates as a function of temperature and aqueous fluid composition. Geochim. Cosmochim. Acta 194, 193–210. https://doi.org/10.1016/j.gca.2016.08.041.
Zheng, C., Bennett, G.D., 2002. Applied Contaminant Transport Modeling, 2nd ed. Wiley Interscience, Canada, p. 621.
Zhu, C., 2003. Coprecipitation in the barite isostructural family: 2. Numerical simulations of reaction and mass transport. Geochim. Cosmochim. Acta 68, 3339–3349. https://doi.org/10.1016/j.gca.2003.10.013.
Dideriksen, K., Zhen-Wu, B.Y., Dobberschütz, S., Rodríguez-Blanco, J.D., Raahauge, P.J., Ataman, E., Oelkers, E.H., Stipp, S.L.S., in prep. A model for nucleation and growth for use in 1 PHREEQC: prediction of barite formation in an oil well.